

Dissection of neuronal gap junction circuits that regulate social behavior in *Caenorhabditis elegans*

Heeun Jang^{a,b}, Sagi Levy^{a,b}, Steven W. Flavell^{a,b,1}, Fanny Mende^c, Richard Latham^c, Manuel Zimmer^c, and Cornelia I. Bargmann^{a,b,2}

^aHoward Hughes Medical Institute, The Rockefeller University, New York, NY 10065; ^bLulu and Anthony Wang Laboratory of Neural Circuits and Behavior, The Rockefeller University, New York, NY 10065; and ^cResearch Institute of Molecular Pathology IMP, Vienna Biocenter, 1030 Vienna, Austria

Contributed by Cornelia I. Bargmann, December 28, 2016 (sent for review November 6, 2016; reviewed by Thomas R. Clandinin and William R. Schafer)

A hub-and-spoke circuit of neurons connected by gap junctions controls aggregation behavior and related behavioral responses to oxygen, pheromones, and food in *Caenorhabditis elegans*. The molecular composition of the gap junctions connecting RMG hub neurons with sensory spoke neurons is unknown. We show here that the innexin gene *unc-9* is required in RMG hub neurons to drive aggregation and related behaviors, indicating that UNC-9-containing gap junctions mediate RMG signaling. To dissect the circuit in detail, we developed methods to inhibit *unc-9*-based gap junctions with dominant-negative *unc-1* transgenes. *unc-1(dn)* alters a stomatin-like protein that regulates *unc-9* electrical signaling; its disruptive effects can be rescued by a constitutively active UNC-9::GFP protein, demonstrating specificity. Expression of *unc-1(dn)* in RMG hub neurons, ADL or ASK pheromone-sensing neurons, or URX oxygen-sensing neurons disrupts specific elements of aggregation-related behaviors. In ADL, *unc-1(dn)* has effects opposite to those of tetanus toxin light chain, separating the roles of ADL electrical and chemical synapses. These results reveal roles of gap junctions in a complex behavior at cellular resolution and provide a tool for similar exploration of other gap junction circuits.

innexin | neural circuits | electrical synapses | stomatin | sensory behavior

Electrical synapses and chemical synapses have complementary functions in the nervous system. Separate regulation of electrical and chemical synapses creates multifunctionality in neural circuits, as illustrated in the vertebrate retina, where regulation of electrical synapses rewires information flow at different light levels (1, 2). Electrical synapses also have essential roles in the developing brain, where they regulate the formation of chemical synapses (3–5). In humans, mutations that affect electrical synapses are associated with neurological conditions such as epilepsy, deafness, and peripheral neuropathies (6–8). However, it is difficult to study electrical synapses in detail because there are few simple functional assays or pharmacological tools that selectively target their activity.

The structural components of electrical synapses are intercellular gap junctions consisting of two aligned hemichannels, each composed of six connexin subunits in vertebrates or eight innexin subunits in invertebrates (9–11). The apposition and opening of these hemichannels form a small protein-lined pore that allows bidirectional ionic flow and electrical coupling between two cells (12). Although the ions always flow down their gradients, the opening of gap junctions can be regulated by membrane potential, transjunctional potential, and protein phosphorylation (12). Gap junctions also allow bidirectional flow of ATP and other intracellular metabolites and function in nonexcitable cells as well as neurons and muscle (12).

The nematode *Caenorhabditis elegans* has gap junctions in neurons and in nonneuronal tissues. Its pharyngeal muscles coordinate their contraction through gap junctions; like the vertebrate heart, its body wall muscles use gap junctions to couple their excitability; and its intestinal cells propagate calcium waves through gap junctions to set the digestive rhythm (13–15). In addition, the anatomical wiring diagram of the *C. elegans* nervous

system derived from electron micrographs has ~600 gap junctions among its 302 neurons, representing about 10% of all synapses (16–19). Circuit manipulations and genetic studies indicate that gap junctions are essential in locomotion circuits and escape behaviors (20, 21). For example, the broadly expressed innexin subunits *unc-7* and *unc-9* are required for coordinated locomotion and link command interneurons with motor neurons to balance forward and backward movement states (21, 22), and *unc-7* also mediates electrical coupling between neurons in the gap junction circuit for nose-touch avoidance behavior (23). However, most neuronal gap junctions are solely predicted by electron micrographs and have not been linked to particular genes or functions.

In *C. elegans*, a network of neurons connected by gap junctions regulates aggregation and a suite of related behaviors. *C. elegans* aggregates into social groups or “clumps” under stressed or crowded conditions (24, 25). This behavior is prominent in wild *C. elegans* strains, which aggregate in response to the high ambient oxygen levels that they encounter in the laboratory (24, 26, 27). Early in its laboratory cultivation, the N2 strain of *C. elegans* acquired a gain-of-function mutation in the neuropeptide receptor NPR-1 that reconciled it to high oxygen levels (27). The *npr-1(gf)* mutation suppresses aggregation and oxygen avoidance, remodels pheromone responses, decreases locomotion speed on food, and results in a selective advantage in laboratory growth (26, 28–33). These behaviors are controlled by a hub neuron called RMG, which has gap junctions with sensory neurons that detect ambient oxygen, pheromones, and other environmental cues (28). In wild strains or *npr-1(lf)* mutants, activity of the RMG circuit promotes aggregation and related responses to

Significance

Electrical coupling through gap junctions is an important form of neuronal communication, but methods to interrogate electrical coupling are limited. We identified the UNC-9 gap junction protein (innexin) as an essential component of a circuit that regulates social aggregation and related behaviors in *Caenorhabditis elegans*. By transgenic expression of dominant-negative UNC-1 stomatin and rescue with gain-of-function UNC-9::GFP, we selectively interrogated and restored gap junction coupling between neurons, allowing fine dissection of the neuronal circuit for social behavior.

Author contributions: H.J., M.Z., and C.I.B. designed research; H.J., F.M., and R.L. performed research; S.L. and S.W.F. contributed new reagents/analytic tools; H.J., S.L., M.Z., and C.I.B. analyzed data; and H.J. and C.I.B. wrote the paper.

Reviewers: T.R.C., Stanford University; and W.R.S., MRC Laboratory of Molecular Biology. The authors declare no conflict of interest.

Freely available online through the PNAS open access option.

¹Present address: Picower Institute of Learning and Memory, Department of Brain and Cognitive Sciences, Massachusetts Institute of Technology, Cambridge, MA 02138.

²To whom correspondence should be addressed. Email: cori@rockefeller.edu.

This article contains supporting information online at www.pnas.org/lookup/suppl/doi:10.1073/pnas.1621274114/-DCSupplemental.

oxygen, pheromones, and food. In *N2* animals, high *npr-1(gf)* activity suppresses the RMG circuit and related behaviors.

The gap junctions are attractive candidates for mediating cell communication in the RMG circuit, but their significance is inferred indirectly from their anatomical presence in electron micrographs. Alternative models for RMG signaling are possible, as all neurons in the circuit also have chemical synapses, and *npr-1* also affects gene expression and neuropeptide signaling (32–34). Here we identify the *unc-9* innexin gene as an essential component of the RMG circuit. Using cell-specific manipulation of *unc-9* activity with Cre recombinase and a newly developed dominant-negative *unc-1(dn)* reagent, we define the roles of gap junctions in specific neurons in generating aggregation and related behaviors. These results demonstrate both localized and distributed roles of neuronal gap junctions in mediating complex behaviors.

Results

unc-9-Based Gap Junctions Are Required for Aggregation Behavior.

The anatomical circuit diagram of *C. elegans* suggests that RMG is the hub of a gap junction circuit composed of unidentified

molecular components, probably innexins (Fig. 1A) (16–19, 28). We hypothesized that mutations affecting gap junctions in the RMG circuit would suppress the aggregation phenotype of *npr-1(lf)* mutants. Double mutants were generated between *npr-1(lf)* and 21 of the 25 predicted innexin genes, excluding the innexin genes that are inviable as null mutants, and aggregation behavior was scored in the double-mutant strains (Table S1). This screen identified *unc-9* and *unc-7* as strong suppressors and *inx-4*, *inx-6*, *inx-17*, and *inx-22* as weak suppressors of the *npr-1* aggregation phenotype. An independent study of a different *npr-1(lf)* phenotype, regulated expression of the *srh-234* chemoreceptor gene, also demonstrated a requirement for *unc-9* and *unc-7* (34).

Both *unc-9* and *unc-7* are expressed broadly in the nervous system, and null mutants in these genes have strong locomotion defects; *unc-9* is also expressed in body wall muscles (35–37). To bypass indirect effects of locomotion on aggregation and narrow down sites of *unc-9* action, we targeted *unc-9* using a cell-specific Cre-Lox strategy (Fig. 1B). A transgene with an *unc-9* cDNA flanked by two *loxP* sites under the *unc-9* promoter was introduced into *unc-9 npr-1* double mutants. This transgene fully

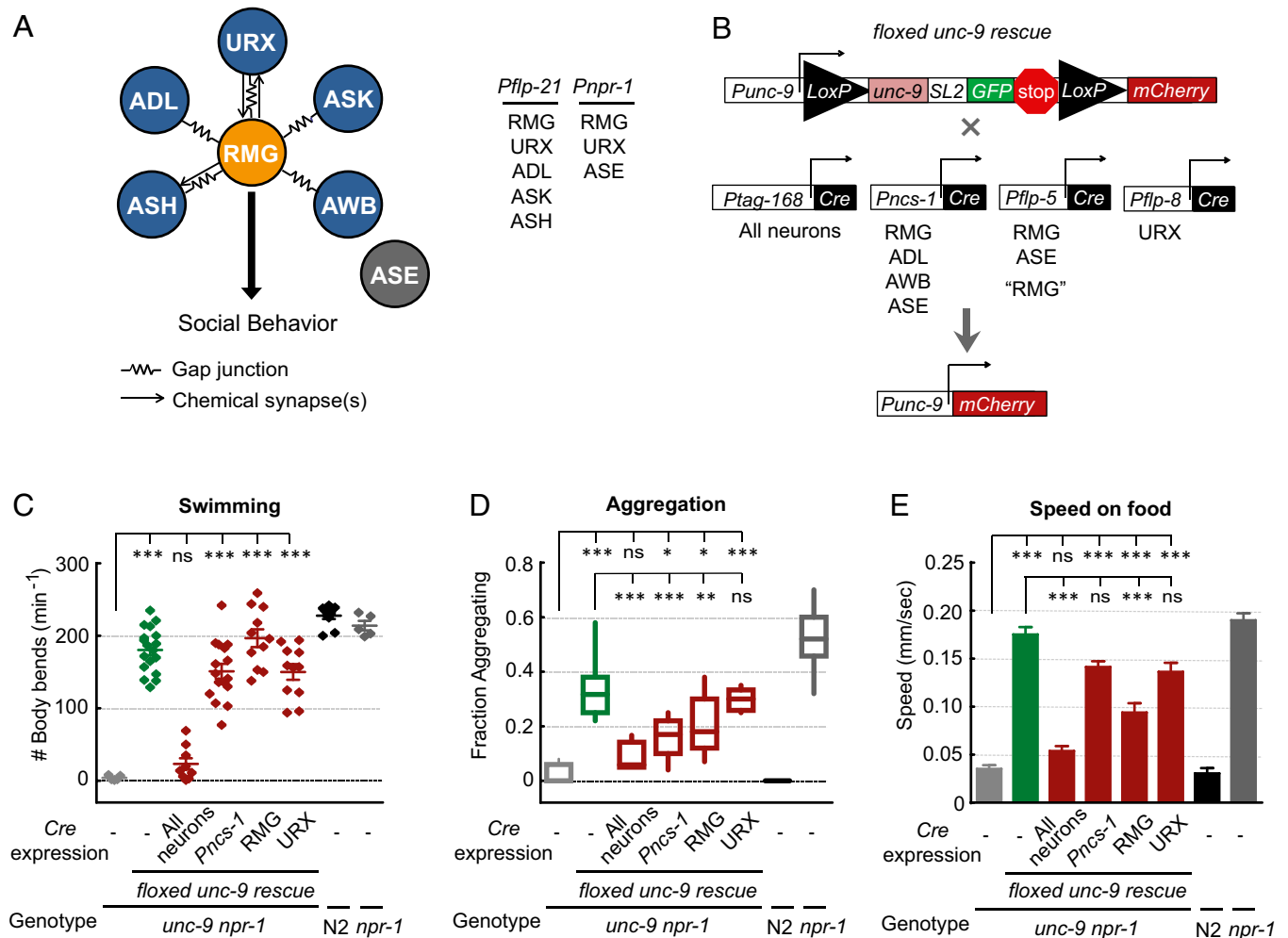


Fig. 1. *unc-9* gap junctions are required for aggregation in *npr-1* mutants. (A, Left) The RMG gap junction circuit for aggregation behavior (16, 17, 19, 28). RMG forms anatomically defined gap junctions with multiple sensory neurons (shown) and some interneurons and motor neurons. (Right) Expression patterns of *npr-1* and *flp-21* promoters used in C–E; complete expression patterns are in Table S3. (B) Cre-Lox reagents for cell-specific knockout of *unc-9* in Cre-Lox strains using *ncs-1*, *flp-5* (“RMG”), and *flp-8* (“URX”) promoters. The *flp-5* promoter drives expression in RMG, ASE, PVT, I4, and M4 neurons and pharyngeal muscles, and the *flp-8* promoter drives expression in URX, AUA, and PVM neurons (see also Table S3). (C) Swimming behavior. Each dot represents the number of body bends per minute measured from a single animal; bars represent mean and SEM. *n* = 5–18 animals per genotype. (D) Aggregation behavior. Boxes represent median and first and third quartiles, and whiskers represent 5th–95th percentiles. *n* = 3–18 assays per genotype. (E) Locomotion speed on a bacterial lawn. Bars represent mean ± SEM. *n* = 2–6 assays per genotype. For all panels, **P* < 0.05, ***P* < 0.01, ****P* < 0.001, ns (nonsignificant) by one-way ANOVA with Dunnett’s correction for multiple comparisons.

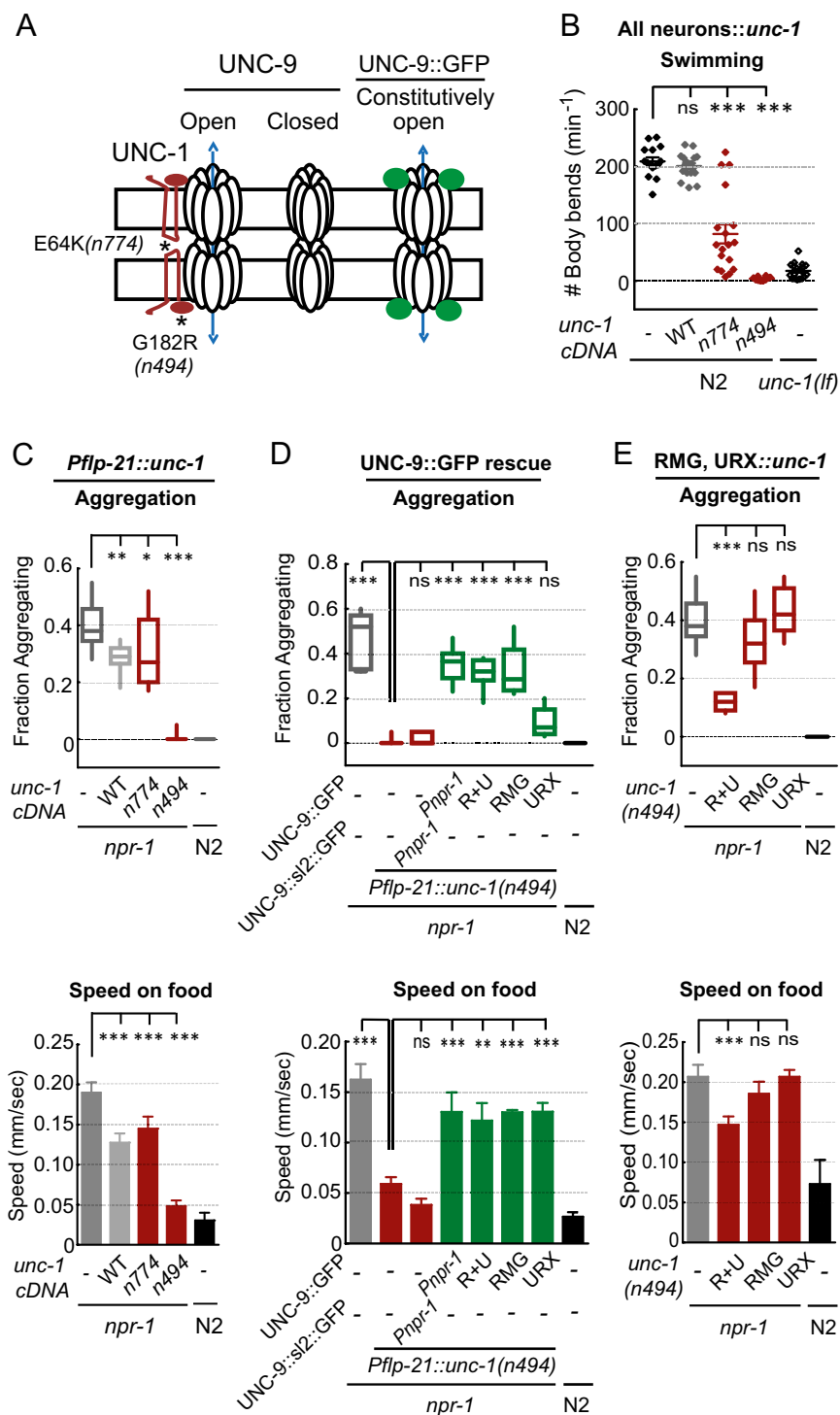


Fig. 2. A dominant-negative *unc-1* cDNA that suppresses aggregation is rescued by UNC-9::GFP. (A) Cartoon of UNC-1 (285 aa) showing location of dominant-negative *n774* and *n494* mutations and its inferred relationship with two aligned gap junction hemichannels composed of eight UNC-9 subunits each from different cells. UNC-9::GFP gap junction can function independently of *unc-1* (37). (B) Swimming behavior in wild-type N2 animals expressing wild-type or mutant *unc-1* cDNAs under the pan-neuronal *tag-168* promoter and in *unc-1*-null mutants. Each dot represents the number of body bends per minute measured from a single animal; bars represent mean and SEM. $n = 10$ –19 animals per genotype. (C) *npr-1* mutants expressing wild-type or mutant *unc-1* cDNAs in the RMG circuit. (Top) Aggregation behavior. $n = 6$ –17 assays per genotype. (Bottom) Locomotion speed in the presence of food. $n = 2$ –8 assays per genotype. (D) *npr-1* mutants expressing *unc-1(n494)* and UNC-9::GFP fusion protein in different subsets of neurons in the RMG circuit. (Top) Aggregation behavior. $n = 5$ –17 assays per genotype. (Bottom) Locomotion speed on a bacterial lawn. $n = 3$ –5 assays per genotype. (E) *npr-1* mutants expressing *unc-1(n494)* cDNA in RMG (*Pflp-5*), URX (*Pflp-8*), or both neurons. (Top) Aggregation behavior. $n = 6$ –10 assays per genotype. (Bottom) Locomotion speed on a bacterial lawn. $n = 3$ –8 assays per genotype. For Top panels in C–E, boxes represent median and first and third quartiles, and whiskers represent 5th–95th percentiles. For Bottom panels in C–E, bars represent mean \pm SEM. For all panels, * $P < 0.05$, ** $P < 0.01$, *** $P < 0.001$, ns (nonsignificant) by one-way ANOVA with Dunnett's correction for multiple comparisons.

rescued locomotion speed in a swimming assay (Fig. 1C, in green) and also rescued aggregation behavior (Fig. 1D, in green; controls in Fig. S1). Therefore, the transgene is expressed at the sites essential for locomotion and aggregation. Expression of Cre recombinase under cell-specific promoters was then used to eliminate *unc-9* activity in targeted cells (*Materials and Methods*). Pan-neuronal deletion of *unc-9* with a *tag-168::Cre* transgene resulted in locomotion defects and a loss of aggregation, suggesting that the observed *unc-9* effects are mediated by neurons (Fig. 1C and D). Deletion of *unc-9* in several neurons of the RMG circuit with a *ncs-1::Cre* transgene suppressed aggregation but allowed normal locomotion (Fig. 1C and D). Suppression of aggregation was also observed after selectively targeting RMG with a *flp-5::Cre* transgene (RMG::Cre; Fig. 1D) but not after targeting URX with a *flp-8::Cre* transgene (URX::Cre; Fig. 1D). Other than RMG, the only site of overlap of *ncs-1* and *flp-5* is the ASE sensory neuron, which is not predicted to form gap junctions in the wiring diagram (16, 19) (Fig. 1A and B). Although the Cre recombinase might be expressed in additional neurons that we did not detect, these results strongly suggest that RMG-specific deletion of *unc-9* gap junctions suppresses aggregation behavior while preserving locomotion.

npr-1 animals have a high crawling speed on a bacterial lawn compared with N2 animals, a foraging behavior that is regulated by the RMG circuit (28). Foraging speed was intermediate between N2 and *npr-1* when floxed *unc-9* was deleted from RMG (Fig. 1E). This result suggests that *unc-9* acts in RMG as well as other neurons to regulate locomotion speed on food.

A Dominant-Negative *unc-1* Mutation Suppresses Aggregation in an *unc-9*-Dependent Manner. *unc-9* has strong genetic interactions with a second gene, *unc-1*, whose mutation leads to a similar uncoordinated and anesthesia-resistant phenotype (38). *unc-1* encodes a stomatin-like integral membrane protein that colocalizes with UNC-9 proteins and modulates the gating of UNC-9 gap junctions in muscle (Fig. 2A) (37). Although most alleles of *unc-1* are recessive, a few are dominant and might be dominant-negative alleles (39). To examine this possibility, we cloned cDNAs for two *unc-1* alleles, *n774* and *n494*, and expressed them pan-neuronally in a wild-type background. Both *unc-1(n774)* and *unc-1(n494)* transgenes reduced swimming speeds in buffer (Fig. 2B, in red). The stronger *unc-1(n494)* transgene resembled *unc-1*- or *unc-9*-null mutant animals (Fig. 2B), consistent with its strong phenotype as a genetic mutant (39). These results suggested that *unc-1(n494)* might be able to inhibit *unc-1* or *unc-9* function in specific neurons.

Expressing *unc-1(n494)* broadly in the RMG circuit using the *flp-21* promoter suppressed the aggregation behavior of *npr-1* mutants and their high foraging speed on food, an effect similar to knocking out *unc-9* in those neurons (Fig. 2C). Locomotion in the *flp-21::unc-1(n494)* strain was normal in the absence of food, indicating that the transgene did not disrupt motor function (Fig. S2A). Expressing *unc-1(wt)* or *unc-1(n774)* cDNAs under the same promoter only slightly decreased aggregation and speed on food (Fig. 2C). Thus, transgenic *unc-1(n494)* interferes with the RMG circuit in ways that resemble inactivation of *unc-9*.

Previous studies demonstrated that an UNC-9::GFP fusion protein can bypass the endogenous function of *unc-1* in body wall muscles, apparently by generating constitutively active gap junctions (37). We found that expressing the UNC-9::GFP fusion protein reversed the effect of the *unc-1(n494)* transgene in *npr-1* mutants and restored aggregation behavior and high locomotion speed (Fig. 2D). In a control experiment, a bicistronic *unc-9::SL2::GFP* transgene that generated separate UNC-9 and GFP protein products did not restore aggregation behavior (Fig. 2D). These results suggest that *unc-1(n494)* suppresses aggregation by inhibiting *unc-9* and not by causing general neuronal defects. Conversely, the behavioral effects of UNC-9::GFP were only

observed in the *unc-1(n494)* context; expressing UNC-9::GFP in an N2 background under either of two promoters did not elicit aggregation behavior, nor did expressing UNC-9::GFP in the *npr-1* background alter aggregation (Fig. S2D). Thus, UNC-9::GFP did not hyperactivate the RMG circuit on its own or interfere with *npr-1* function. The mutual dependence of *unc-1(n494)* and UNC-9::GFP supports a close interaction between these genes.

UNC-1 is a regulatory subunit and not a structural subunit of gap junctions, and the sites of *unc-1(n494)* activity were not always identical to those identified for *unc-9* in the Cre-Lox experiments. In general, *unc-1(n494)* had to be expressed in a greater number of cells to have an effect, suggesting that it might attenuate function best when expressed by both gap junction-coupled neurons. For example, Cre-Lox deletion of *unc-9* in RMG suppressed aggregation in *npr-1* animals (Fig. 1D), but expression of *unc-1(n494)* from the same promoter did not (Fig. 2E). However, expressing *unc-1(n494)* simultaneously in the oxygen-sensing URX neurons and the RMG neuron suppressed aggregation (Fig. 2E), in agreement with previous studies suggesting that RMG and URX both contribute to this behavior (28).

Rescue with UNC-9::GFP provided a view of the contributing neurons that was more similar to *unc-9* knockout. Expressing the UNC-9::GFP fusion protein in RMG neurons was sufficient to rescue aggregation in the *flp-21::unc-1(n494)* strain, but expression in URX was not (Fig. 2D). Although there are subtleties, the results of these manipulations consistently point to RMG as the site at which *unc-9* and *unc-1(n494)* exert their strongest effects on aggregation.

Locomotion speed on food was strongly suppressed by *unc-1(n494)* expression from the *flp-21* promoter, and this effect was rescued by expressing UNC-9::GFP in either RMG or URX (Fig. 2D). However, locomotion speed was only weakly suppressed by *unc-1(n494)* expression in both RMG and URX (Fig. 2E). This intermediate result resembles the intermediate effects of cell-specific *unc-9* knockout on locomotion (Fig. 1E) and indicates that RMG, URX, and other *flp-21*-expressing neurons regulate locomotion speed on food.

Cell-Specific Expression of *unc-1(n494)* in the RMG Circuit Modifies Individual Sensory Behaviors. Previous experiments with the RMG circuit have examined the effects of silencing sensory transduction with *tax-4* or *osm-9* mutations or silencing synaptic transmission with a tetanus toxin light chain (24, 28, 40). The *unc-1(n494)* transgene presented an opportunity to ask where gap junctions might act to regulate individual aggregation-related behaviors, which was pursued by expressing *unc-1(n494)* alone or in combination with UNC-9::GFP using different cell-specific promoters.

Aggregation in *npr-1* animals is strongly associated with avoidance of high oxygen levels (26). The URX neurons sense increasing oxygen concentrations directly and are required for behavioral responses to oxygen upshifts that include reversals, turning, and increased locomotor speed (31, 41, 42). Expressing *unc-1(n494)* in the RMG circuit with the *flp-21* promoter shifted the oxygen-dependent locomotion speed and reversal rates of *npr-1* animals toward those of N2 animals (Fig. 3A–D). The effects of *unc-1(n494)* on speed were partly reversed by expressing UNC-9::GFP either in the URX or in the RMG neurons or in both (Fig. 3A–D). These results suggest that oxygen responses are regulated by gap junctions in several neurons of the RMG circuit, including RMG, URX, and other *flp-21*-expressing neurons.

The activity of the URX sensory neurons is regulated by oxygen, but this primary sensory response has not been compared between N2 and *npr-1* animals. Using functional calcium imaging, we did not detect significant differences in URX oxygen responses when comparing N2, *npr-1*, and *unc-1(n494)* strains

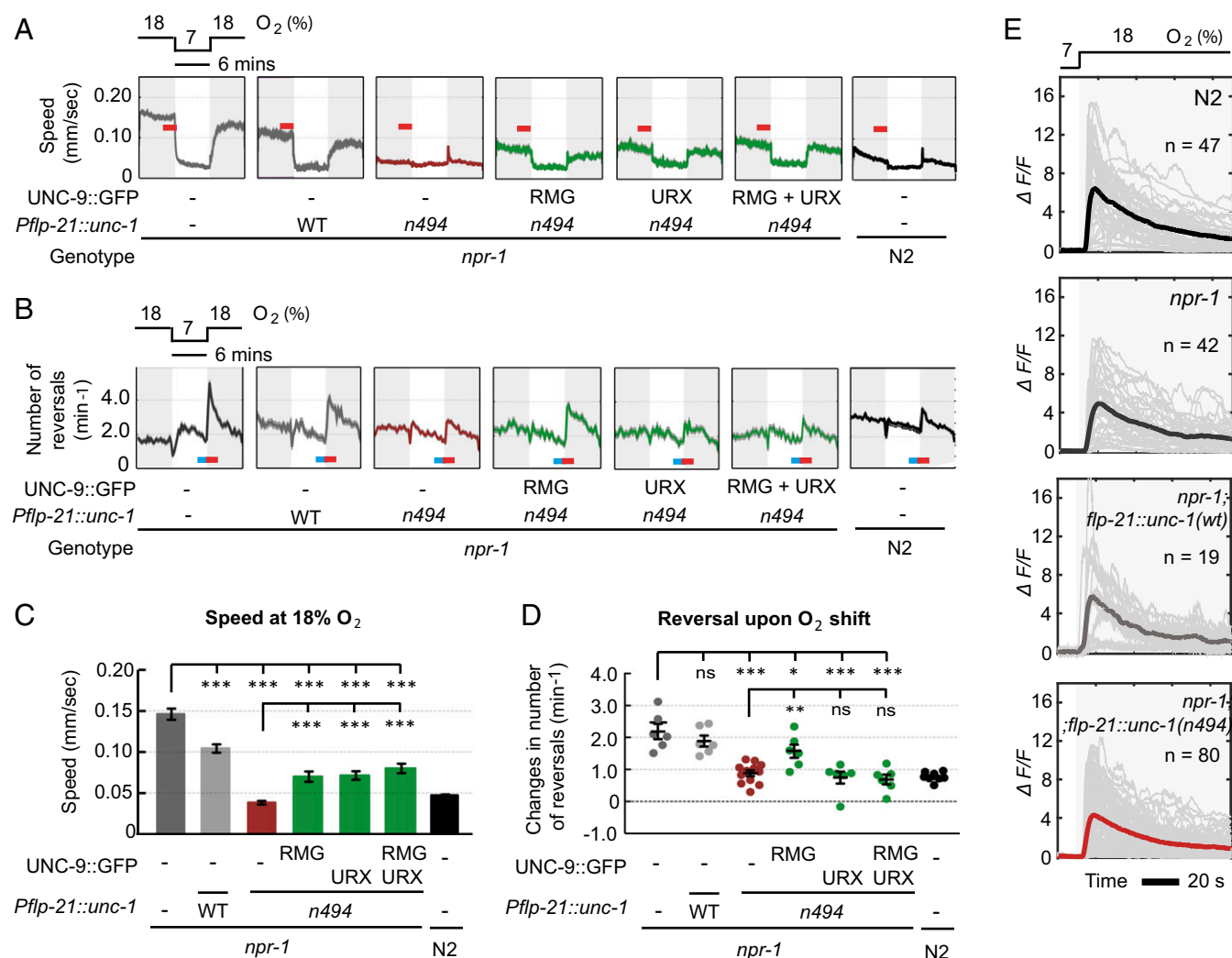


Fig. 3. Gap junction signaling in the RMG circuit is required for *npr-1* modulation of O_2 chemosensory responses. (A) Population mean locomotion speed (\pm SEM) in response to an 18%–7%–18% oxygen switch. Red bars indicate the 80-s time windows used for quantification in B, and gray areas indicate periods at 18% oxygen. (B) Population mean frequency of reversal initiation events (\pm SEM) in response to a 18%–7%–18% oxygen switch. Red and blue bars indicate the time windows compared for quantification in D, and gray areas indicate periods at 18% oxygen. (C) Trial means of locomotion speed (\pm SEM) at 18% oxygen represented as bar graphs. (D) Trial means of reversal frequency change (post–pre) (\pm SEM) in response to a 7%–18% oxygen switch from the same experiments. (E) Calcium imaging of URX in response to oxygen upshift (7%–18%). Mean and individual traces are shown as black and gray lines, respectively. Traces show *G-CaMP5K* fluorescence relative to baseline (mean fluorescence from 1 to 10 s). Genotypes and number of animals are indicated in each panel. Data in A and C are binned by 1 s and 15 s, respectively. Each trial was performed on ~50–90 animals. $n = 6$ trials, except $n = 8$ for N2 and $n = 12$ for *npr-1; Pflp-21::unc-1(n494)*. Population mean is an average across all recorded animals in each bin. Trial mean is the average of population means from each trial calculated from the periods indicated by red bars in A and C. * $P < 0.05$, ** $P < 0.01$, *** $P < 0.001$, ns (nonsignificant) by one-way-ANOVA with Holm–Sidak’s multicomparison correction.

under conditions similar to the ones at which these strains had distinct behaviors (Fig. 3E). Although more detailed analysis may yield differences in URX calcium responses, these results suggest that oxygen-sensitive behavior might be regulated by *npr-1* and gap junctions at a step downstream of or parallel to the initial URX calcium response (33).

In another *npr-1*-regulated behavior, N2 animals are repelled by the pheromone *ascr#3* (*asc- Δ C9*), but *npr-1* animals are not (Fig. 4A–C) (43). *ascr#3* is sensed by the ADL neurons in the RMG circuit (43). Expressing *unc-1(n494)* in ADL in *npr-1* animals caused them to avoid *ascr#3* (Fig. 4C, in red), as did expressing *unc-1(n494)* in either RMG or URX (Fig. 4D and E). As URX does not form any direct gap junctions with ADL, this result suggests that *ascr#3* avoidance may reflect both direct and indirect effects of the RMG gap junctions on ADL-mediated behaviors (16, 17, 19). Control experiments demonstrated that a

unc-1(wt) cDNA had no effect on *ascr#3* avoidance (Fig. 4C–E) and that *unc-1(n494)* expression did not enhance *ascr#3* avoidance in an N2 background (Fig. S3A).

In examining additional candidates from the RMG circuit, we found that expressing *unc-1(n494)* in ASK neurons significantly reduced locomotion speed on food, like *unc-1(n494)* expression in RMG and URX (Fig. 4F). However, expressing *unc-1(n494)* in ASK did not reduce speed off food or aggregation (Fig. 4G and H).

unc-1(n494) also had little effect on aggregation when expressed simultaneously in ASH and ADL, two neurons whose sensory activity is required for *npr-1*-related behaviors (Fig. S3B) (24). However, simultaneous manipulation of chemical synapses in ASH and ADL reciprocally increased or suppressed aggregation, suggesting that these neurons interact with aggregation behavior through their chemical synapses (Fig. S3C).

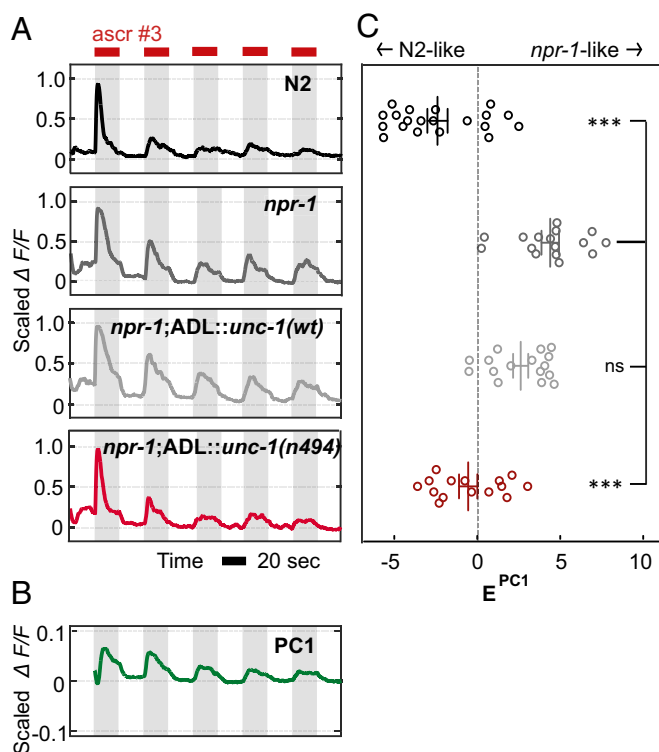


Fig. 5. ADL calcium responses to *ascr#3* in *unc-1(n494)* strains. (A) Average calcium responses detected with *G-CaMP5K* in N2, *npr-1*, *npr-1;ADL::unc-1(wt)*, and *npr-1;ADL::unc-1(n494)* animals. Each trace was scaled to its maximum value F_{max} before averaging (Materials and Methods). Gray areas indicate five 20-s pulses of 100 nM *ascr#3* (*asc-ΔC9*). $n = 20$ animals for N2, 16 for *npr-1*, 16 for *npr-1;ADL::unc-1(wt)*, and 15 for *npr-1;ADL::unc-1(n494)*. (B) Visual representation of the first principal component explaining 32% of the variance in 10 tested genotypes (Fig. S5). (C) PCA of ADL calcium responses. The graph shows the distribution of eigenvalues of the first principal component (E^{PC1}) in each genotype, with mean value and SEM. Each dot represents an eigenvalue from a single trace. *** $P < 0.001$, ns (nonsignificant) by one-way ANOVA with Dunnett's correction for multiple comparisons.

ADL calcium responses were highly variable between animals with the same genotype, and even between individual *ascr#3* pulses (Fig. S4). This variability could be due to genetic, environmental, or technical differences between the experiments. To better understand the features of the ADL response that might vary between genotypes, we used principal component analysis (PCA) to analyze a full ADL imaging dataset from 10 different strains (Fig. S5 and Materials and Methods). Intuitively, the aim of this approach was to extract filters that best separated the input traces and subsequently ask whether such unbiased filters were preferentially associated with particular genotypes. Each principal component represents a time course that explains a fraction of the variance between traces. The first principal component identified in this analysis explained 32% of the total variance between traces, followed distantly by the second (11%) and third (7.2%) components (Fig. S5D).

Direct inspection of the first principal component indicates that it largely reflects the rate of adaptation in the calcium response within and between *ascr#3* pulses (Fig. 5B and Fig. S5E). Reconstruction of traces based on the eigenvalues of the first principal component supported that conclusion (Fig. S4), and statistical analysis of its eigenvalues identified a substantial and significant separation of N2 and *npr-1* traces based on genotypes (Fig. 5C and Materials and Methods).

Expression of *unc-1(n494)* in ADL, RMG, or URX neurons of *npr-1* animals resulted in a significant shift toward N2-like responses

in this first principal component, matching the behavioral result (Fig. 5A and B and Fig. S5). In control experiments, expressing *unc-1(wt)* in ADL or URX had no effect, although *unc-1(wt)* did have a partial effect when expressed in RMG (Fig. S5A and B). ADL expression of *unc-1(n494)* or *unc-1(wt)* in the N2 background did not alter ADL responses, consistent with the behavioral data indicating that *unc-1(n494)* only affects *npr-1* animals (Fig. S5A and B). Together, these results suggest that the first principal component in this analysis represents features of the ADL calcium response that are significantly affected by the *npr-1* genotype and similarly affected by *unc-1(n494)*. The observed effect on ADL adaptation is reminiscent of the role of *npr-1* in the ASH neurons, where it enhances adaptation to noxious stimuli (45).

Discussion

The innexin encoded by *unc-9* is essential in the RMG hub-and-spoke circuit that regulates aggregation, foraging speed on food, and behavioral responses to oxygen and pheromones. The genetic requirement for an innexin provides functional support for the model of the RMG circuit suggested by the *C. elegans* wiring diagram, whose central feature is the communication of multiple sensory neurons with an RMG hub through gap junctions. Chemical synapses of many neurons also modify these behaviors (28), demonstrating that gap junctions and chemical synapses in the RMG circuit have complementary rather than redundant roles.

After demonstrating an effect of *unc-9* in the RMG circuit, we showed that a dominant-negative *unc-1(n494)* transgene can antagonize the function of UNC-9-containing gap junctions. The rescue of *unc-1(n494)* by UNC-9::GFP supports a close link between *unc-1* and *unc-9* in the RMG circuit. Further use of *unc-1(n494)* transgenes may help to establish the roles of *unc-9* gap junctions in other circuits and may be useful to bypass the strong locomotion defect in *unc-9*-null mutants. Such studies should, however, include the UNC-9::GFP control to exclude off-target effects. The specificity of *unc-1* is not known, and it might also interact with gap junctions encoded by other *C. elegans* innexins. Even within the RMG circuit, *unc-9* is not the only candidate innexin; RMG expresses *unc-7*, and ADL and ASK express *inx-18* (35). Moreover, although stomatin proteins such as UNC-1 can regulate electrical synapses in *C. elegans*, the family has other functions. Some *C. elegans* and vertebrate stomatin proteins are regulators of ENaC/Deg channels, and most stomatins are uncharacterized (37, 46, 47). Future studies will determine whether UNC-1 selectively and specifically modulates electrical synapses.

The expression of *unc-1(n494)* in the RMG circuit had a dramatic effect on aggregation and related behavior in *npr-1* mutants but no significant effect on N2 animals. Therefore, *unc-1(n494)* interacts specifically with the *npr-1*-sensitive features of the RMG circuit and its component neurons; it does not, for example, interfere with the basic oxygen-sensing properties of URX or pheromone-sensing properties of ADL. NPR-1 is a G protein-coupled receptor thought to be coupled to the Gi/o pathway, but its ultimate molecular target is not known (30, 48). It is possible that NPR-1 regulates UNC-9-containing gap junctions directly, but it might also silence the RMG circuit by affecting excitability, synaptic transmission, or neuropeptide signaling (28, 33, 34, 49).

The importance of *unc-9/unc-1*-sensitive gap junctions varied considerably among different neurons, depending on the relevant behaviors. Aggregation behavior was closely associated with *unc-9* activity in the RMG neuron, consistent with its identity as a hub neuron and its many gap junctions, and also included a contribution from URX neurons. The regulation of locomotion speed was distributed among several neurons, including RMG, URX, and ASK. Sensory responses to oxygen levels also involved RMG, URX, and other neurons. Some of these responses are rapidly modified by acute expression of *npr-1* from a heat shock

promoter, suggesting that they are acute and primary readouts of circuit activity (40, 43).

The results of these experiments help to distinguish between alternative models of RMG circuit function. For example, ASH and ADL have been proposed to act as current sinks for RMG that only indirectly contribute to the function of the RMG circuit (33). However, *unc-1(n494)* interference with gap junctions, which would be expected to negate this function, did not suppress aggregation, and modulation of their synaptic output could affect aggregation bidirectionally, suggesting an instructive role for these neurons. That said, the genetic results are consistent with many possibilities, and a full understanding awaits fast and direct assays for gap junctions and synaptic activity *in vivo*.

Ascr#3 pheromone avoidance was sensitive to *unc-1(n494)* expression at multiple locations, including ADL, RMG, and the indirectly connected URX neuron. Thus, both direct and indirect effects of *npr-1* on ADL are mediated by the RMG circuit. In another example of an *npr-1*-dependent but indirect effect, expression of the ADL chemoreceptor gene *srh-234* is indirectly regulated by *unc-7* and *unc-9* expression in other neurons (34) and is likely to represent a slow pathway for reconfiguring the circuit. *npr-1* mutants show an altered gene expression landscape at the whole-animal level affecting neuropeptides, insulin signaling, and metabolic processes that are important during embryonic and larval development (32). The chronic behavioral state induced by *npr-1* may alter circuit physiology and gene expression over a variety of spatial and temporal scales, which may be more easily resolved with new tools for manipulating gap junctions.

Materials and Methods

Genetics. In Cre-Lox experiments (Fig. 1 and Fig. S1), two separate transgenes were made by microinjection and then crossed with one another to generate animals bearing both transgenes that were tested for behavior. This design was used to prevent recombination or transactivation between the tested plasmids. Cell-specific expression of Cre recombinase and subsequent elimination of *unc-9* activity was verified by the absence of GFP and/or the presence of mCherry in targeted cells. A full strain list appears in Table S2.

In most cases, transgenic strains were coinjected with *Pmyo-3::mCherry* (5 ng/μL), *Punc-122::dsRed* (20–25 ng/μL), or *Punc-122::GFP* (10–25 ng/μL).

ADL imaging strains were coinjected with *Psre-1::tagRFP* (50 ng/μL), and URX imaging strains were coinjected with *Pflp-8::mCherry* (2 ng/μL). Empty pSM vector was added to bring the total concentration of injected DNA to 60–100 ng/μL.

Molecular Biology.

Coding sequences. The wild-type *unc-1* cDNA was amplified by RT-PCR from total N2 RNA. Primers used for amplification were 5'-attattagCTAGGatgtcaacaacaggaagaacaga-3' and 5'-attattagGGTACctattggtcttttccataaagtctcc-3', and the resulting PCR product was cloned into the pSM-SL2::GFP vector via the NheI and KpnI sites. This 858 bp-long cDNA translates into UNC-1 isoform A with 285 amino acids. To generate mutant cDNAs of *unc-1*, the wild-type *unc-1* construct was mutated using overlap extension PCR. For the *n774* mutation, the 178th nucleotide was mutated to introduce the E64K mutation. For the *n494* mutation, the 544th nucleotide was mutated to introduce the G186R mutation.

The 1,164 kb-long *unc-9* cDNA codon-optimized for *C. elegans* expression (a generous gift from Loren Looger, Howard Hughes Medical Institute Janelia Campus, Ashburn, VA) was used for floxed *unc-9* rescue and expression of *unc-9::SL2::GFP*. For expression of *unc-9::GFP* fusion protein, an *unc-9::GFP* fragment (a generous gift from Zhao-Wen Wang, University of Connecticut, Farmington, CT) (37) was cloned into the pSM vector via the XbaI and NheI sites.

G-CaMP5Kopt was modified for optimal codon use in *C. elegans* using the OptimumGene method (GenScript).

Promoters. To drive the expression of floxed *unc-9* rescue construct, 9 kb upstream, the start codon of *unc-9* was amplified from the genomic DNA of N2 animals and cloned into the pSM vector using the FseI and AscI sites. Oligonucleotides used for cloning were 5'-attataGGCCGGCCagaagaatagctctgcatatgatgtcttg-3' and 5'-attaatGGCGCCcctaagtcattgctgacgcg-3'.

In other transgenes, the following promoters were used: *npr-1* promoter (7,196 bp), 5'-CTCAGTCTCGTGTG-3' and 5'-TTTTTGTAGTCTAATGGAGGA-3';

flp-5 promoter (4,250 bp), 5'-AAAGATTACAAGTGACGTGA-3' and 5'-GGCTTGCAACTGGCTCCG-3'; *sre-1* promoter (1,000 bp), 5'-GTCACACGAGTGT-3' and 5'-GTTGGAATGAAAA-3'; and *srh-220* promoter (2,449 bp), 5'-GGTGATAGATAGACCGTCC-3' and 5'-ACTTGAGTTGGACCGAAAA-3'.

tag-168, *ncs-1*, *flp-21*, *flp-8*, *sra-9*, and *sra-6* promoters were as described (28, 50).

Behavioral Assays. GraphPad Prism software was used for all statistical analyses. Primary behavioral data appears in Dataset S1.

Swimming behavior. A single animal was picked using minimal amount of bacterial food and gently transferred into a well filled with a drop of 50 μL M9 in a 96-well plate. Animals started thrashing immediately after transfer. After 1 min, the number of complete body bends was counted by eye for the following 1-min period to generate thrashing rate per minute.

Aggregation and bordering behavior. Assays were performed simultaneously as described (25, 27). Assay plates were prepared with a circular lawn about 10 mm in diameter by seeding 50 μL *Escherichia coli* OP50 on an NGM plate and growing for 4 d at room temperature. Sixty young adult animals grown at room temperature were picked onto the off-food area of the assay plate, and the aggregating and bordering were scored after 1 h. Aggregation was measured by calculating the fraction of animals that are in contact with two or more animals along at least half of their body length. Bordering was measured by calculating the fraction of animals that resided within 2 mm of the edge of the bacterial lawn. Fraction aggregating or bordering obtained was then analyzed with one-way ANOVA with Dunnett's correction for multiple comparisons. For *inx-6(rr5);npr-1(ad609)* mutants, animals were grown at room temperature and incubated overnight at 25 °C, the restrictive temperature for *rr5* temperature-sensitive allele, before being assayed at 25 °C.

Locomotion speed. Speed was measured as described (50). Twenty to thirty young adult animals were transferred onto a food-free assay plate or a food assay plate with a uniform *E. coli* OP50 lawn grown overnight at room temperature. Animals were allowed to crawl freely within a 28 mm × 28 mm arena confined by a filter paper soaked with 10 mM CuCl₂ solution. At 30 min after transfer, the arena was recorded for 5–10 min. Video recordings were made at 3 frames per second using a Pixellink camera and Streampix software, followed by analysis with custom software written in MATLAB (Mathworks). Mean speed was obtained from each assay plate with 20–30 animals, and values from two to eight independent assay plates were averaged to generate data for each genotype and condition.

Oxygen flow behavioral assays. Locomotion responses to changing O₂ concentrations were determined in a population behavioral assay as described previously (41, 51) with some modifications. For preparation of assay plates, 14 cm-diameter NGM plates were inoculated with a dense solution of *E. coli* OP50 bacteria and left for 1 d at room temperature to yield a homogeneous bacterial lawn. A 56 mm × 56 mm assay arena was defined by a Whatman paper soaked with 20 mM CuCl₂, a repellent, to prevent animals from leaving the arena. Fifty to ninety adult animals were transferred to the arena and left unperturbed for 1 h. At 5 min before recording onset, a transparent Plexiglas device with a flow arena of 56 mm × 56 mm × 0.7 mm was placed on top of the assay arena. O₂ concentrations were controlled using a static gas mixer connected to mass flow controllers (Vögtling Instruments) operated by LabView software. Total gas flow was set to 100 mL/min. During illumination with a red flat LED, animals were recorded at 3 frames per second using a 4 megapixel CCD (Jai) camera and Streampix software. Movie analysis, speed measurements, and turn detection were performed using a modified MATLAB-based tracking software (52), available at med.stanford.edu/wormsense/tracker/. For speed calculation, only periods of continuous forward movement were used and data were binned by taking the mean of three consecutive frames (1-s binning). Reversal initiation events were detected by measuring characteristic changes in angular velocity, and data were binned by taking the sum of events in 45 consecutive frames (15-s binning). The event frequency (min⁻¹) was calculated for each bin. For quantifications, we accounted for experiment-to-experiment variation by calculating trial means; that is, for each individual experiment, the population means within the indicated time windows were calculated.

Acute pheromone avoidance. *Ascr#3* (*asc-ΔC9*) was a generous gift from Rebecca Butcher, University of Florida, Gainesville, FL. The drop test assay was performed essentially as described to address acute avoidance of pheromone (53). All assays were performed in the presence of food, on uniform *E. coli* OP50 lawn on NGM plates (100 mm × 15 mm) that were grown overnight at 37 °C. Young adult animals that were grown in room temperature were transferred to the assay plate at room temperature to equilibrate for 30–60 min. We delivered 25 nM of *ascr#3* prepared in M13 buffer (30 mM Tris, pH 7.5, 100 mM NaCl, 10 mM KCl) by mouth-pipetting to individual animals

moving forward via a 10- μ L glass capillary that was previously pulled by laser-based micropipette puller (P-2000, Sutter Instrument) and whose tip was gently broken. Responses were scored as reversals if animals initiated backward movements longer than half their body length within 4 s. Effect sizes (shown in figures as fraction reversing) represent the increase or decrease in fraction of animals reversing in response to pheromone, compared with the fraction reversing in response to M13 buffer alone.

ADL calcium imaging and PCA. For ADL imaging, transgenic animals expressed *G-CaMP5K* sequence-optimized for expression in *C. elegans* under the ADL-specific *sre-1* promoter. Animals were imaged in custom-fabricated polydimethylsiloxane (PDMS) chamber (54). A single well-fed animal was loaded onto the chamber and allowed to equilibrate for 5 min, followed by photo-bleaching for 2 min before imaging to silence the light response of ADL. We prepared 10 mM ascr #3 (asc- Δ C9) in ethanol stored at -20°C at 100 nM in S-basal buffer (stimulus), and the equivalent amount of ethanol was prepared in S-basal buffer (nonstimulus control). Stimuli were delivered by using a vacuum system and automated switching between two fluid streams with a three-way valve, a ValveBank controller, and Metamorph software. Each animal was imaged once. Image stacks were obtained at 10 frames per second using an Andor iXon3 camera, Metamorph Software, and a 40 \times objective on the Zeiss Axioplan microscope. Stacks were then processed with a custom-written script using ImageJ. A first-level analysis of traces indicated no difference in maximum $\Delta F/F0$ response between N2 and *npr-1*. However, variations in transgene expression and a low basal fluorescence level compared with background autofluorescence generated apparent $\Delta F/F0$ values that varied widely between traces of each genotype. To minimize this effect of transgene expression, all traces were individually normalized on a 0 to 1 scale. The median values of responses during 50–60, 90–100, 130–140, 170–180, and 210–220 s (the last 10 s of second to sixth off-stimuli) were used as *F0* baseline and normalized *F* values to generate $\Delta F/F0$.

PCA was performed across ADL calcium traces from 10 genotypes (shown in Fig. S5) using a custom MATLAB script. All calcium traces individually scaled on a 0 to 1 axis were subjected to PCA over the time domain so that each principal component represents a time vector. Time points beginning 2 s before the first ascr#3 stimulus through 20 s after the last ascr#3 stimulus

were used for PCA (total 202 s). The eigenvalues of the first principal component (E^{PC1}) were compared between different genotypes by ANOVA. Reconstruction in Fig. S4 was made by (mean) + (E^{PC1}) \times (PC1).

URX calcium imaging and analysis. Ca^{2+} imaging of URX neurons was performed using a microfluidic device for controlling environmental O_2 levels as described previously with some modifications (31, 41, 42). Animals were imaged in the presence of *E. coli* OP50 bacteria suspended in S-basal at 0.6 OD, to mimic on-food conditions that were used in the behavioral assays, and 1 mM of the muscle paralyzing compound tetramisole, to fully suppress movement. O_2 concentrations were controlled with a static gas mixer connected to mass flow controllers (Vögtling Instruments) operated by LabView software. Total gas flow at the inlet to the device was set to 50 mL/min. Fluorescence of *G-CaMP5K* expressed in URX was recorded with an inverted epifluorescence microscope equipped with a CoolLED pE-2 excitation system (470 nm) and Piston GFP bandpass filter set. Imaging data were acquired with a Photometrics Evolve 512 EMCCD camera with 100 ms exposure time, streaming images at 10 Hz acquisition rate to VisiView software. Fluorescence intensity time series were extracted from the image sequences using a custom-written script in Metamorph software. A region of interest (ROI) and a neighboring background region in each frame was defined based on thresholding and tracked using the Metamorph track objects function, the total integrated fluorescence intensity of the ROI was determined, and background fluorescence was subtracted in each frame. We report and quantify the fluorescence relative to a baseline: $\Delta F/F = (F - F0)/F0$. *F0* is the median fluorescence within 1–99 s from recording onset.

ACKNOWLEDGMENTS. We thank Rebecca Butcher for purified ascr#3, Loren Looger for *GCaMP* and the *unc-9* cDNA, and Zhao-Wen Wang for *UNC-9::GFP*. This work was funded by the Howard Hughes Medical Institute and by a grant from the Ellison Medical Foundation (to C.I.B.), by a Human Frontiers Science Program Fellowship (to S.L.), and by the European Community's Seventh Framework Programme (FP7/2007-2013)/ERC Grant Agreement Number 281869 (acronym: elegansNeurocircuits) (to M.Z.). C.I.B. was an investigator of the Howard Hughes Medical Institute.

- Baldrige WH, Ball AK, Miller RG (1987) Dopaminergic regulation of horizontal cell gap junction particle density in goldfish retina. *J Comp Neurol* 265(3):428–436.
- Li H, et al. (2013) Adenosine and dopamine receptors coregulate photoreceptor coupling via gap junction phosphorylation in mouse retina. *J Neurosci* 33(7):3135–3150.
- Pereda AE (2014) Electrical synapses and their functional interactions with chemical synapses. *Nat Rev Neurosci* 15(4):250–263.
- Hormuzdi SG, Philippov MA, Mitropoulou G, Monyer H, Bruzzone R (2004) Electrical synapses: A dynamic signaling system that shapes the activity of neuronal networks. *Biochim Biophys Acta* 1662(1-2):113–137.
- Chuang CF, Vanhoven MK, Fetter RD, Verselis VK, Bargmann CI (2007) An innexin-dependent cell network establishes left-right neuronal asymmetry in *C. elegans*. *Cell* 129(4):787–799.
- Martinez AD, Acuña R, Figueroa V, Maripillan J, Nicholson B (2009) Gap-junction channels dysfunction in deafness and hearing loss. *Antioxid Redox Signal* 11(2):309–322.
- Carlen PL, et al. (2000) The role of gap junctions in seizures. *Brain Res Brain Res Rev* 32(1):235–241.
- Wei CJ, Xu X, Lo CW (2004) Connexins and cell signaling in development and disease. *Annu Rev Cell Dev Biol* 20:811–838.
- Oshima A, Matsuzawa T, Murata K, Tani K, Fujiyoshi Y (2016) Hexadecameric structure of an invertebrate gap junction channel. *J Mol Biol* 428(6):1227–1236.
- Unwin PN, Ennis PD (1984) Two configurations of a channel-forming membrane protein. *Nature* 307(5952):609–613.
- Unger VM, Kumar NM, Gilula NB, Yeager M (1999) Three-dimensional structure of a recombinant gap junction membrane channel. *Science* 283(5405):1176–1180.
- Goodenough DA, Paul DL (2009) Gap junctions. *Cold Spring Harb Perspect Biol* 1(1):a002576.
- Starich TA, Lee RY, Panzarella C, Avery L, Shaw JE (1996) *eat-5* and *unc-7* represent a multigene family in *Caenorhabditis elegans* involved in cell-cell coupling. *J Cell Biol* 134(2):537–548.
- Li S, Dent JA, Roy R (2003) Regulation of intermuscular electrical coupling by the *Caenorhabditis elegans* innexin *inx-6*. *Mol Biol Cell* 14(7):2630–2644.
- Peters MA, Teramoto T, White JQ, Iwasaki K, Jorgensen EM (2007) A calcium wave mediated by gap junctions coordinates a rhythmic behavior in *C. elegans*. *Curr Biol* 17(18):1601–1608.
- White JG, Southgate E, Thomson JN, Brenner S (1986) The structure of the nervous system of the nematode *Caenorhabditis elegans*. *Philos Trans R Soc Lond B Biol Sci* 314(1165):1–340.
- Xu M, et al. (2013) Computer assisted assembly of connectomes from electron micrographs: Application to *Caenorhabditis elegans*. *PLoS One* 8(1):e54050.
- Jarrell TA, et al. (2012) The connectome of a decision-making neural network. *Science* 337(6093):437–444.
- Varshney LR, Chen BL, Paniagua E, Hall DH, Chklovskii DB (2011) Structural properties of the *Caenorhabditis elegans* neuronal network. *PLoS Comput Biol* 7(2):e1001066.
- Chalfie M, et al. (1985) The neural circuit for touch sensitivity in *Caenorhabditis elegans*. *J Neurosci* 5(4):956–964.
- Kawano T, et al. (2011) An imbalancing act: Gap junctions reduce the backward motor circuit activity to bias *C. elegans* for forward locomotion. *Neuron* 72(4):572–586.
- Starich TA, Xu J, Skerrett IM, Nicholson BJ, Shaw JE (2009) Interactions between innexins UNC-7 and UNC-9 mediate electrical synapse specificity in the *Caenorhabditis elegans* locomotory nervous system. *Neural Dev* 4:16.
- Chatzigeorgiou M, Schafer WR (2011) Lateral facilitation between primary mechanosensory neurons controls nose touch perception in *C. elegans*. *Neuron* 70(2):299–309.
- de Bono M, Tobin DM, Davis MW, Avery L, Bargmann CI (2002) Social feeding in *Caenorhabditis elegans* is induced by neurons that detect aversive stimuli. *Nature* 419(6910):899–903.
- de Bono M, Bargmann CI (1998) Natural variation in a neuropeptide Y receptor homolog modifies social behavior and food response in *C. elegans*. *Cell* 94(5):679–689.
- Gray JM, et al. (2004) Oxygen sensation and social feeding mediated by a *C. elegans* guanylate cyclase homologue. *Nature* 430(6997):317–322.
- McGrath PT, et al. (2009) Quantitative mapping of a digenic behavioral trait implicates globin variation in *C. elegans* sensory behaviors. *Neuron* 61(5):692–699.
- Macosko EZ, et al. (2009) A hub-and-spoke circuit drives pheromone attraction and social behaviour in *C. elegans*. *Nature* 458(7242):1171–1175.
- Cheung BH, Cohen M, Rogers C, Albayram O, de Bono M (2005) Experience-dependent modulation of *C. elegans* behavior by ambient oxygen. *Curr Biol* 15(10):905–917.
- Rogers C, et al. (2003) Inhibition of *Caenorhabditis elegans* social feeding by FMRFamide-related peptide activation of NPR-1. *Nat Neurosci* 6(11):1178–1185.
- Busch KE, et al. (2012) Tonic signaling from O_2 sensors sets neural circuit activity and behavioral state. *Nat Neurosci* 15(4):581–591.
- Andersen EC, Bloom JS, Gerke JP, Kruglyak L (2014) A variant in the neuropeptide receptor *npr-1* is a major determinant of *Caenorhabditis elegans* growth and physiology. *PLoS Genet* 10(2):e1004156.
- Laurent P, et al. (2015) Decoding a neural circuit controlling global animal state in *C. elegans*. *eLife* 4:e04241.
- Gruner M, et al. (2014) Feeding state, insulin and NPR-1 modulate chemoreceptor gene expression via integration of sensory and circuit inputs. *PLoS Genet* 10(10):e1004707.
- Altun ZF, Chen B, Wang Z-W, Hall DH (2009) High resolution map of *Caenorhabditis elegans* gap junction proteins. *Dev Dyn* 238(8):1936–1950.
- Liu Q, Chen B, Gaier E, Joshi J, Wang ZW (2006) Low conductance gap junctions mediate specific electrical coupling in body-wall muscle cells of *Caenorhabditis elegans*. *J Biol Chem* 281(12):7881–7889.
- Chen B, Liu Q, Ge Q, Xie J, Wang ZW (2007) UNC-1 regulates gap junctions important to locomotion in *C. elegans*. *Curr Biol* 17(15):1334–1339.

